J. Phys. Chem. A **2002,** *106,* 10063−10071

ARTICLES

Irradiated Guanine: A Car-Parrinello Molecular Dynamics Study of Dehydrogenation in the Presence of an OH Radical

Christopher J. Mundy,* Michael E. Colvin,† and Andrew A. Quong

Chemistry and Materials Science, Lawrence Livermore National Laboratory, Livermore, California 94550, and Biology and Biotechnology Research Program, Lawrence Livermore National Laboratory, Livermore, California 94550

Received: May 24, 2002; In Final Form: August 2, 2002

Understanding the basic chemistry of the interaction of radicals with DNA bases is imperative when trying to elucidate the potential effects of radiation on DNA. Experimental evidence points to guanine as having the highest affinity of all the DNA bases for undergoing damage. In this study we use Car-Parrinello molecular dynamics (CPMD) in conjunction with traditional quantum chemical methods to research the possible mechanisms for the gas-phase damage of guanine in the presence of an OH radical. Our findings indicate that, for most of the sampled starting configurations, dehydrogenation of guanine (to yield guanine radical and water) is spontaneous *and* free energetically most favored at all hydrogen sites except at C8. Furthermore, through state-of-the-art analysis, we are able to separately track the nuclear and electronic rearrangement during the dehydrogenation reactions, and find examples of both concerted and stepwise abstraction of the proton and electron. We also find spontaneous hydroxylation at C8 and C4 in accordance with experimental findings.

Introduction

The interaction of radiation with biological macromolecules such as DNA is a complex process involving both direct interaction of radiation with the macromolecule and indirect interactions via unstable radicals formed by irradiation of smaller compounds, primarily water. While full scale modeling of radiation interacting with the cell is formidable, it is possible to simulate the initial physical interactions of radiation with DNA via the Monte Carlo method.[1−3] Generally speaking, these studies simulate the single-scatter electron transport through water, as well as diffusion of free radicals to the DNA, record the number and character of damage events, and empirically convert damage events into single- and double-strand breaks. Although Monte Carlo methods are shown to be feasible, one drawback is their inability to predict molecular damage to the DNA base from the radical.

Understanding the basic chemistry of radicals and DNA bases is an important step in characterizing the potential damage to DNA. The chemical-level understanding of such damage has far-reaching implications for radiation therapy, health effects of radiation exposure, and aging.[4] The complex problem of experimentally determining the precise nature of DNA damage currently addresses only selected aspects of this question. One class of experimental studies use crystals of DNA bases where techniques such as electron spin resonance are used to elucidate the products after the crystal is subjected to intense radiation.[5−8] The complexity of interpreting such data has given a unique opportunity for quantum chemists to perform calculations on individual DNA bases to shed light on the relative stability of radical structures and compute the hyperfine coupling constants to help interpret experimental data.[8−13] Other experimental studies have elucidated the nature of base damage through direct chemical reactions of DNA bases with oxidizing agents. Here, investigators have observed different products of the oxidative process depending on both the oxidizing reagent and conditions under which the reaction takes place.[14−22]

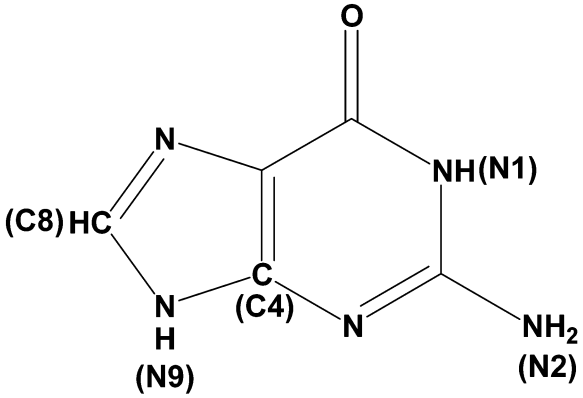

Figure 1. Schematic of the guanine molecule. Parenthetical labels refer to the dehydrogenation and hydroxylation sites.

It has long been known that guanine (see Figure 1) has the highest affinity of all the DNA bases for undergoing oxidation. Thus, we chose to study guanine in the presence of an OH radical. This investigation will allow us to consider the relative propensities for hydroxylation and dehydrogenation of the DNA

---

* Corresponding author.

† Biology and Biotechnology Research Program.

10.1021/jp0212904 CCC: $22.00

base, both of which have been experimentally observed. The possible reaction products arising from these reactions have been researched and characterized in many recent experimental efforts.[14−22] A theoretical investigation characterized possible irradiated products of various DNA bases.[9,10] These potential products are categorized by common chemical modification (e.g., hydrogenation, dehydrogenation, hydroxylation) and within each category the possible radical products are ranked in terms of their relative stability. A more recent theoretical study investigated the pK_a of cation radicals of various DNA bases in connection with proton-coupled electron-transfer mechanisms that have been observed in recent experiments.[23] Calculations have also gone beyond the single base to include the effects of hydrogen bonding and stacking on radical stabilization.[8,24] All of the aforementioned studies have involved characterization of the electronic structures of the reactants and products of guanine oxidation. Our aim is to use molecular dynamics to theoretically deduce possible reaction mechanisms for the initial steps of the gas-phase oxidation of guanine in the presence of an OH radical.

To perform molecular dynamics studies of reaction mechanisms it is essential to use quantum mechanical force fields. Thus, we choose to use Car-Parrinello molecular dynamics (CPMD)[25,26] to elucidate the possible mechanisms of radical formation in DNA bases. Since the seminal paper by Car and Parrinello, CPMD has found great success as a tool in chemistry and materials science. CPMD is a density functional theory-based method that solves the Kohn−Sham equations[27] in the pseudo-potential approximation using a plane-wave basis. The efficiency of the CPMD method lies in the fact that the electronic degrees of freedom are treated as dynamical variables and can be updated "on-the-fly." Studies have shown that density functional theory with gradient-corrected functionals yields accurate results for many chemical properties.[28]

The use of the plane-wave basis is by far the easiest to numerically implement. However, because of its generality, plane-waves often do not provide an intuitive picture that lends itself to a chemical interpretation. Great strides to alleviate this problem came with the development of maximally localized Wannier functions.[29−31] Wannier functions are localized functions obtained by a constrained unitary transformation of the original Kohn−Sham eigenstates. The constraint is often, but not limited to, the Boys criteria for obtaining localized orbitals.[32] Incorporating the efficient calculation of the Wannier centroids (WCs) as the CPMD progresses have proven to be a useful tool in deducing subtle changes in electronic structure on the reaction mechanisms.[33,34] Again, the evolution of the WCs within the Boys localization condition proves invaluable in the present study.

Although there have been many great successes using the CPMD method, static ab initio quantum chemical methods have complementary strengths including the ability to exactly characterize stationary points on the potential energy surface, the ability to easily calculate thermal and entropic corrections to the molecular energy, and the availability of a hierarchy of levels of theory and methods for partitioning the electron distribution. Even within density functional theory, the use of Gaussian basis sets in quantum chemical methods allows the easy inclusion of exact electron exchange. Hence, in this study we have used both conventional Gaussian basis quantum chemical methods as well as CPMD. This allows us to relate our calculations to published quantum chemical studies and to compare different levels of theory (dependence on basis set and exchange-correlation functional) resulting in a more complete picture of possible reaction mechanisms of an irradiated DNA base.

Methods

CPMD was implemented in a plane-wave basis within local spin density approximation (LSDA) functional theory with an energy cutoff of 70 Rydbergs and with Becke exchange and Lee−Yang−Parr (BLYP) gradient-corrected functional.[35,36] Norm conserving pseudo-potentials were used for oxygen, hydrogen, nitrogen, and carbon.[28,37] The CPMD dynamics were performed in the constant energy ensemble (NVE) in an isolated cubic cell of length 13.229 Å using the Poisson solver of Martyna and Tuckerman.[38] WCs were calculated every five time-steps using the algorithm of Berghold et al.[31] In the CPMD simulations, each time-step corresponds to 5.0 au.

The Gaussian basis set quantum chemical calculations were performed using density functional theory with the Becke three parameter exchange and Lee−Yang−Parr correlation functional (B3LYP).[36,39] Several basis sets where used in the calculations. The molecular geometries were optimized with the 6-31++G-(3df,3pd) basis set. The molecular entropies and thermal corrections to the free energies were calculated from the harmonic vibrational constants determined by analytic energy second derivatives calculated at the optimized B3LYP/6-31G**. For the single point atomic charge calculations on snapshots from the CPMD simulations a 6-31++G** basis was used.

The transition states for the dehydrogenation reactions were optimized at the B3LYP/6-31G** level of theory and verified to be the saddle points for the proper reaction by analysis of the analytical B3LYP/6-31G** harmonic vibrational frequencies. The energies of the transition states were determined from single point B3LYP/6-31++G(3df,3pd) energy calculations at the B3LYP/6-31G** optimized geometries. (Using the geometries optimized with the smaller basis set was found to have a negligible effect on the energies of the reactants and products as compared to optimizations using the larger basis set.)

For comparison with earlier published data we also calculated the B3LYP/6-311G(2df,p) energies at the B3LYP/6-31G** optimized geometries. The atomic charges were calculated using natural population analysis (NPA).[40] Unrestricted wave functions were used for open shell molecules (all doublets); in all cases the resulting S^2 eigenvalue was very close to the exact value. We reoptimized the unrestricted B3LYP/6-31G** structures using the restricted open shell wave function with the same basis set and DFT functional. (The restricted results lowered the energies of the N1, N9, and C8 radicals relative to N2 by 0.4, 1.1, and 1.3 kcal/mol, respectively, but did not alter the ordering of the structures.)

To estimate the effect of aqueous solvation on the relative energies, single point energies were calculated at the B3LYP optimized geometries using a dielectric continuum solvation model (COSMO[41]) coupled to the B3LYP/6-31++(3df,3pd) wave functions. All calculations were done using Gaussian 98.[42]

Results and Discussion

Quantum Chemical Studies of Hydroxyl Reactions with Guanine. The relative free energies of the four doublet-state dehydrogenation products of guanine are listed in Table 1. Results are given for both the gas phase and the aqueous phase (as modeled by the continuum solvation model). In the gas phase the N2 is the most favored dehydrogenation site, followed by the N9 site (1.9 kcal/mol) and the N1 site (3.4 kcal/mol), with the C8 site strongly unfavored (26.9 kcal/mol). Use of a much smaller 6-31G** basis set and exclusion of the zero-point

TABLE 1: Relative Energies of Dehydrogenated Guanine Radicals in Units of kcal/mol Calculated Using Different Methods[a]

	B3LYP/G-31++G(3df,3pd)// B3LYP/G-31++G(3df,3pd)				B3LYP/ 6-311G(2pd,p)// 6-31G**	CPMD
	electronic energy	enthalpy (0°)	free energy (298°)	aqueous phase free energy (298°)	enthalpy (0°)	energy
N1	4.71	4.03	3.40	1.65	4.43	3.73 ± 0.53
N2	0.00	0.00	0.00	2.56	0.00	0.00 ± 0.94
N9	2.75	2.26	1.88	0.00	2.62	3.13 ± 0.41
C8	26.67	26.87	26.74	25.98	26.76	25.72 ± 0.62

[a] The corrections for enthalpy and free energy were calculated from the B3LYP/6-31G** harmonic vibrational frequencies, and the solvation effects were calculated using the COSMO model. The B3LYP/6-311G(2pd,p)//B3LYP/6-31G** energies were calculated for comparison with the earlier results of Wetmore et al.

TABLE 2: Reaction and Transition Barrier Enthalpies and Free Energies for the Dehydrogenation and Hydroxylation of Guanine by Hydroxyl Radical[a]

product	reaction enthalpy	reaction enthalpy barrier	reaction free energy	reaction free energy barrier
N1-dehydrogenated guanine	−24.21	not located	−26.11	not located
N2-dehydrogenated guanine	−28.72	−7.49	−29.52	0.86
N9-dehydrogenated guanine	−26.04	−7.78	−27.63	0.15
C8-dehydrogenated guanine	−1.51	1.48	−2.77	9.64
C4-hydroxylated guanine	−17.47	none	−7.35	none
C8-hydroxylated guanine	−31.17	none	−21.68	none

[a] All energies calculated at the B3LYP/6-31++(3df,3pd)//B3LYP/6-31G** level of theory and the enthalpy and free energy corrections were determined from the B3LYP/6-31G** harmonic vibrational frequencies. The negative reaction barriers indicate that the transition states are lower in energy that the infinitely separated reagents.

energy, thermal, and entropic corrections do not alter this energy ordering. Inclusion of the aqueous solvation effects narrows the range of relative energies and alters this ordering so that the N9 site is the most favored dehydrogenation site, followed by N1 (1.7 kcal/mol) and N2 (2.6 kcal/mol) and C8 (26.0 kcal/mol). The change in the relative energy of the N2 site is due to the smaller predicted solvation energy of the N2 product.

Table 2 lists the enthalpies and free energies for the dehydrogenation and hydroxylation reactions, as well as the enthalpies and free energies of the reaction transition state if they exist. For the dehydrogenation reactions, the predicted enthalpies are similar to the free energies and are negative, indicating that dehydrogenation at the N1, N2, N9, and C8 sites on guanine are all energetically favored. For the hydroxylation reactions at C4 and C8, the reaction free energies are ∼10 kcal/mol less favored than the reaction enthalpies. This difference is due to the entropic cost of a reaction in which two reactants combine to form a single product (in contrast to the dehydrogenation in which two reactants form two products). This entropic effect is large enough to alter the relative reaction free energies of the reactions studied. Although the C8 hydroxylation is the most enthalpically favored, the reaction free energies favor dehydrogenation at the N1, N2, and N9 positions. This is an interesting observation given the current experimental literature on the solution-phase chemistry of the initial steps of guanine oxidation. For oxidizing agents other than an OH radical, there seems to be some evidence that oxidation of guanine proceeds directly through a guanine radical cation.[15,16,22] When one considers the solution chemistry of the OH radical and guanine, the observations seem to indicate that C8 hydroxylation is strongly favored.[17,19,43] There is also evidence that oxidation of guanine can occur via the guanine cation with OH radical as the oxidizing agent.[19] However, experiment seems to indicate that this mechanism of guanine oxidation proceeds through a C4-hydroxylated intermediate.[19] According to Table 2, the C4-hydroxylated radical is the *least* stable of the radicals we studied in the gas phase—one motivation to examine possible reaction mechanisms within CPMD.

The transition state structures and energies were calculated for the dehydrogenation reaction at the N2, N9, and C8 sites. The search for a transition state barrier for the N1 dehydrogenation was complicated by the close proximity of the OH radical to one of the N2 hydrogens. In all attempts to locate the transition state for the N1 dehydrogenation, the hydroxyl radical instead abstracted the N2 hydrogen. No transition states were found for the hydroxylation at the C4 and C8 positions. This result was verified by constrained optimizations at every 0.1 Å along the reaction coordinate (the C—OH distance).

For the dehydrogenations at the N2 and N9 positions, we find negligible reaction free energy barriers so that these reactions will happen spontaneously even at very low temperature. For the dehydrogenation at the C8 position we predict a 9.6 kcal/mol reaction barrier, indicating that this reaction would occur at a reasonable rate at room temperature, but would be slow at very low temperature.

In a recent study by Wetmore et. al.,[9] similar density functional gas-phase calculations were performed with a Gaussian basis set using B3LYP/6-31G** geometry optimizations followed by B3LYP/6-311G(2df,p) single point energy calculations; and reported 0° enthalpies (total energies with zero-point energy corrections).[9] These authors find slightly different results predicting N9-dehydrogenation to be the most favorable followed by N1- and N2-dehydrogenation being roughly equal approximately 2 kcal/mol higher relative to the N9 site. C8-dehydrogenation was the least favorable, approximately 24 kcal/mol higher in energy than the N9 site. We find that the results obtained with the same basis set and DFT functional as used by Wetmore et. al.[9] yield relative energies in close agreement with our larger basis set results, and in slight disagreement with those published by Wetmore.

Table 3 lists the predicted electron affinities of the guanine radical cation and the OH radical in both the gas and aqueous

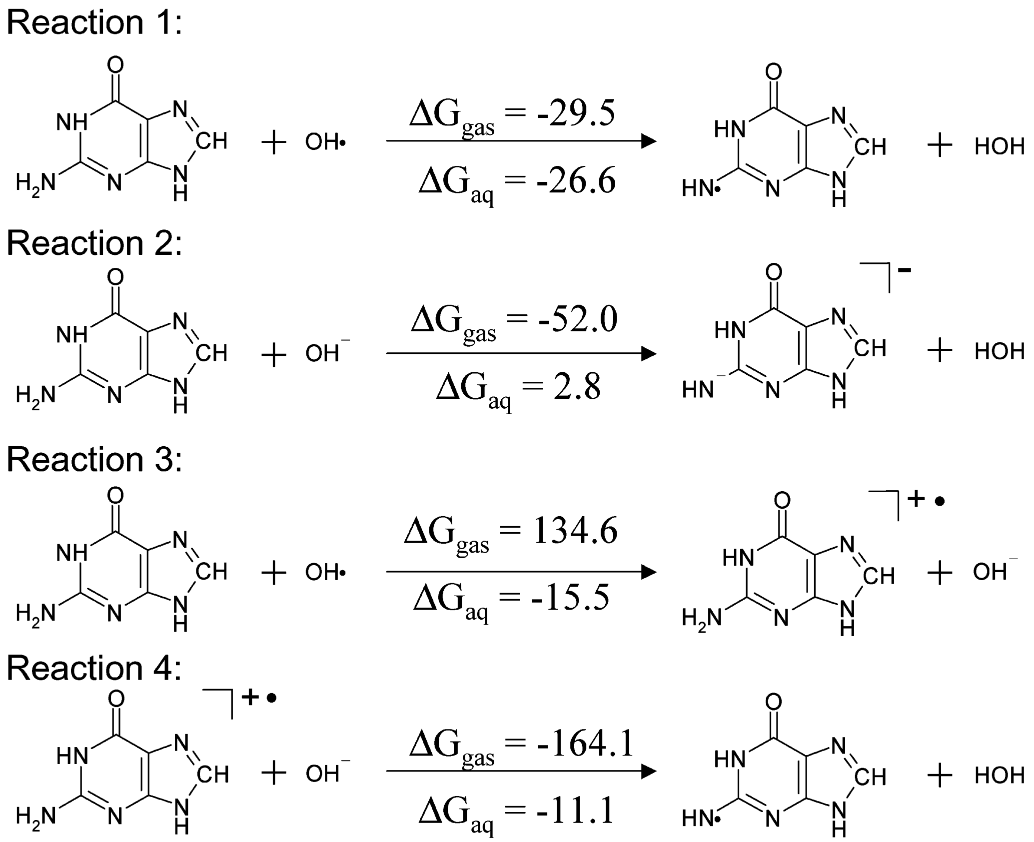

Figure 2. Gas- and aqueous-phase reaction energies of guanine and hydroxide radicals in kcal/mol. Energies calculated at the B3LYP/6-31++G-(3df,3pd)//B3LYP/6-31++G(3df,3pd) level of theory; solvation effects included using the COSMO solvation model.

TABLE 3: Electron Affinities and Solvation Energies for Selected Species in kcal/mol[a]

	gas-phase E.A. (expt result in parentheses)	aqueous phase E.A.	ΔG_{solv}
guanine			−22.99
guanine radical cation	175.09 (181)[b]	126.84	−71.25
OH anion			−106.43
OH radical	40.50 (42.2[c])	142.31	−4.61

[a] The energies were calculated at the B3LYP/6-31++G(3df,3pd)//B3LYP/6-31++G(3df,3pd) level of theory. The corrections for free energy were calculated from the B3LYP/6-31G** harmonic vibrational frequencies, and the solvation effects were calculated using the COSMO model. [b] Ref 45. [c] Ref 46.

phases, as well as the solvation free energy for the guanine radical cation, neutral guanine, OH anion, and OH radical. The good agreement between the experimental and predicted electron affinities indicate that the Gaussian basis set used is sufficient to accurately describe these different electronic states. Also, the free energies of aqueous solvation are listed in Table 3.

As previously discussed, the possibility of electron exchange between the guanine and the OH radical gives this system a rich reaction chemistry. Figure 2 shows a series of possible reactions at the N2 site between guanine and OH. Reaction 1 is the direct abstraction of the N2 hydrogen by the OH radical to yield water and a guanine radical. This reaction is strongly favored and has nearly identical predicted reaction free energies in the gas and aqueous phases—indeed a strong justification for studying the details of this reaction in the gas phase. In strong contrast, the corresponding deprotonation (reaction 2) by an OH anion has very different gas- and aqueous-phase energetics, with the reaction being nearly 55 kcal/mol more favorable in the aqueous phase than in the gas phase. This difference arises from the much higher solvation energy of the OH anion (−106. kcal/mol) compared to that of the guanine anion (−69 kcal/mol). It is clear that the details of this reaction are best suited for being studied in solvent.

Reactions 3 and 4 are the components of a possible two-step mechanism for reaction 1. The first step (reaction 3) is the abstraction of an electron, followed by the abstraction of the N9 proton by the hydroxyl anion (reaction 4). Note that this energy analysis assumes that the products of reaction 3 fully separate before recombining in reaction 4 and that there is sufficient time for the electronic state of the guanine radical formed by electron abstraction in reaction 3 to relax to the lowest energy state for the guanine cationic doublet radical. These assumptions are not necessary in the CPMD simulations of this process described below. The predicted energies show that the initial electron abstraction is very unfavorable in the gas phase, due to the much higher gas-phase electron affinity of the guanine radical cation versus the OH radical (see Table 3). In the aqueous phase, however, these reaction energies are dramatically altered (due to the large solvation energy of the OH anion) so that both reactions 3 and 4 have strongly negative reaction free energies.

The large differences between the gas and condensed phase energetics of reaction 3 in Figure 2 provides another motivation for our CPMD simulations. As will be discussed below with the CPMD results, there are intermediate conditions between the gas phase and the fully solvated aqueous phase. For example, in reaction 3 the very unfavorable energy of charge separation in the products would be mitigated if the products remained associated in an ion pair. However, characterizing such ion pairs is extremely difficult using conventional quantum chemical methods because the resulting structures have very floppy geometries, or may not even correspond to a local minimum on the potential energy surface. A motivation is that the CPMD simulations can also effectively simulate reactions involving a very rapid sequence of steps in which the time scale for the relaxation of the electronic wave function determines the rate of steps in the mechanism, for example the electron transfer and subsequent proton transfer in the dehydrogenation at the guanine N2 position. Hence, to elucidate whether a complete or partial electron-transfer precedes the hydrogen shift, dynamical simulations of the reaction must be performed.

Car-Parrinello Molecular Dynamics of Guanine and Its Radicals. Our CPMD studies involved two types of calculations. First, we determined the relative stability of dehydrogenated guanine radicals and then performed dynamical simulations of the reaction of guanine with an OH radical. To calculate the relative stabilities of the guanine radical within CPMD we first abstracted the hydrogen, followed by a wave function minimization and 0.6 picoseconds of MD to come to thermal equilibrium. We then requenched the wave function and performed an additional 0.6 ps of MD in order to ensure that we were indeed on the Born−Oppenheimer surface. CPMD results are also listed in Table 1. These results show that differences due to basis set (plane-waves used in CPMD versus a very large Gaussian basis set 6-31++G (3df, 3pd)) and the exchange functional (BLYP versus B3LYP) do not significantly affect the results. CPMD and quantum chemical calculations are in good agreement that the most stable guanine radical results from hydrogen extraction from the N2-site followed closely by N9 (3.13 kcal/mol) and N1 (3.73 kcal/mol).

Car-Parrinello Molecular Dynamics of Guanine + OH Radical. Our second set of CPMD calculations involved dynamical simulations of the reaction trajectory of hydroxyl radicals placed at different starting points around the guanine. Such simulations will indicate the likely reaction mechanisms and indicate whether low-barrier reaction paths exist. In these simulations we used four different starting conformations that will be separately discussed below. The goal of these molecular dynamics simulations is to produce a series of reaction paths for guanine reacting with OH radical that are biased only by the choice of starting conditions. Additionally, these results are a first step toward addressing a series of open questions about this reaction. First, what is the effect of the starting configurations on the observed products (relevant since within the DNA helix access to individual atoms within the nucleotide bases is sterically constrained)? Second, are there other possible products that form spontaneously from this reaction? Third, what are the reaction mechanisms that lead to these predicted products?

As previously mentioned, because CPMD provides the time evolution of the atoms and the WCs it is uniquely suited to study the detailed mechanisms of these reactions. Ideally, one should explore a vast number of initial configurations that could give rise to different chemical reactions in order to ascertain the dependence of initial conditions on reaction mechanisms and products. Even the fastest parallel computers do not yet allow the exploration of the full phase space of initial conditions, so in this study we chose to simulate only those chemical reactions resulting from configurations in which the OH radical begins within 2 Å of each possible site of dehydrogenation, and a "facial" configuration in which the OH radical was centered above the plane of the guanine molecule. The results of these simulations are described below.

Facial OH Attack. We placed the OH radical 4 Å above the plane formed by the relaxed guanine structure. This geometry places the OH radical roughly equidistant (4.5 Å from the N2 and N9 sites (see Figure 3). From the initial state shown in Figure 3 we performed the CPMD calculations. We find a rapid dehydrogenation (within one picosecond) at the N2 site (see Figure 1) to form the guanine radical and water. This product is consistent with relative stabilities of the possible dehydrogenation products presented in Table 2. Furthermore, if one examines the total Kohn−Sham energy as a function of time, the difference from the reactant to product (26.98 kcal/mol) agrees with that calculated for reaction 1 in Figure 2 (for which the gas- and aqueous-phase energies are nearly equal). This energy is then converted into translational and vibrational energy in the resulting products. This observation manifests itself in the high kinetic energies of the ions and electrons in the CPMD simulation. A more detailed examination of N2 dehydrogenation will follow below.

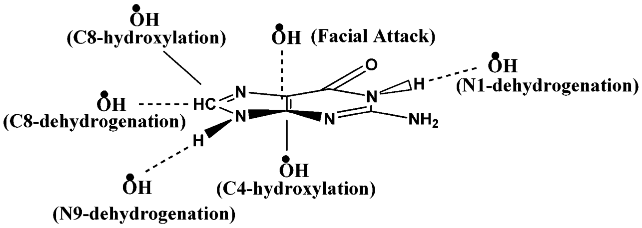

Figure 3. Schematic of the different initial conditions explored in the CPMD simulations. The parenthetical labels refer to the corresponding reactions as described in the text. Dashed lines represent CPMD runs that were initiated without prior geometry optimization. Solid lines denote a prior geometry optimization before the CPMD dynamics were initiated.

C8 Dehydrogenation. We begin with the reaction with the OH radical 2 Å from the C8 dehydrogenation site (see Figure 3). After 2 ps of CPMD there is seemingly no propensity for dehydrogenation of guanine at C8, instead the OH radical simply floats in front of the C8 hydrogen at H−O distance of about 2.5 Å, a somewhat longer distance than the 1.5−2.0 Å of a typical hydrogen bond. The C8 hydrogen abstraction to form the guanine radical and an H_2O is predicted by our calculations to have a reaction free energy of −2.8 kcal/mol. Although predicted to be thermodynamically favored, this is a much less exothermic reaction than hydrogen extraction from N1, N2, or N9, and based on this CPMD simulation, apparently has a reaction barrier as corroborated by the Gaussian basis set calculations (see Table 2).

N9 Dehydrogenation. We next examine the reaction with the OH radical 2 Å from the N9 dehydrogenation site as shown in Figure 3. This configuration yields a rapid dehydrogenation reaction at the N9 site within 1 ps. We have analyzed the electronic and nuclear motion during these reactions. The structure from the time-step where the hydrogen is halfway between the N9 and OH is shown in Figure 4. An interesting feature of Figure 4 is that the hydrogen abstraction by the OH occurs without any decrease in the electron density associated with the sigma N9−H bond. Instead the hydrogen abstraction involves a concerted loss of electron density (i.e., a WC) from the conjugated guanine rings. In some of the reactions described subsequently, this electron transfer is not concerted with the hydrogen transfer, but occurs earlier, leading to a partial negative charge on the OH before hydrogen abstraction. Note that in DNA the N9 is the site of the glycosidic linkage to the deoxyribose sugar, so that the N9 dehydrogenation just described would not occur for DNA-bound guanine.

N2 Dehydrogenation. As described above, our results predict that the N2 guanine radical is the most stable of the dehydrogenation products. This is corroborated with the "facial attack" initial configuration shown in Figure 3 which produced spontaneous dehydrogenation at the N2 position. Figure 5 shows

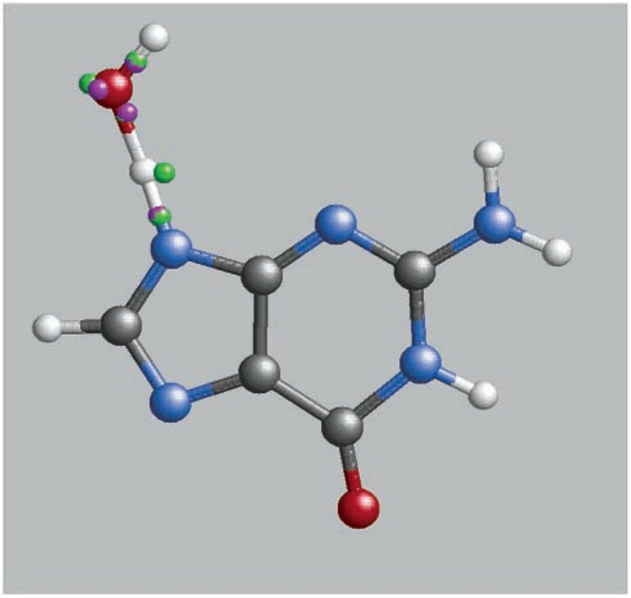

Figure 4. Halfway along the reaction path for the hydrogen abstraction leading to the formation of a guanine radical. Carbon is denoted by gray spheres, nitrogen by blue spheres, oxygen by red spheres, and hydrogen by white spheres. The WCs are depicted by green ("α"-spin) and magenta ("*β*"-spin) spheres. It is clear that the reaction proceeds with the removal of a neutral hydrogen atom from the guanine (white sphere + green sphere). Note that the electron density in N9−H *σ*-bond is still present (overlapping green and magenta spheres near N9). From this angle it is also possible to see the spin-polarized lone pair on the oxygen.

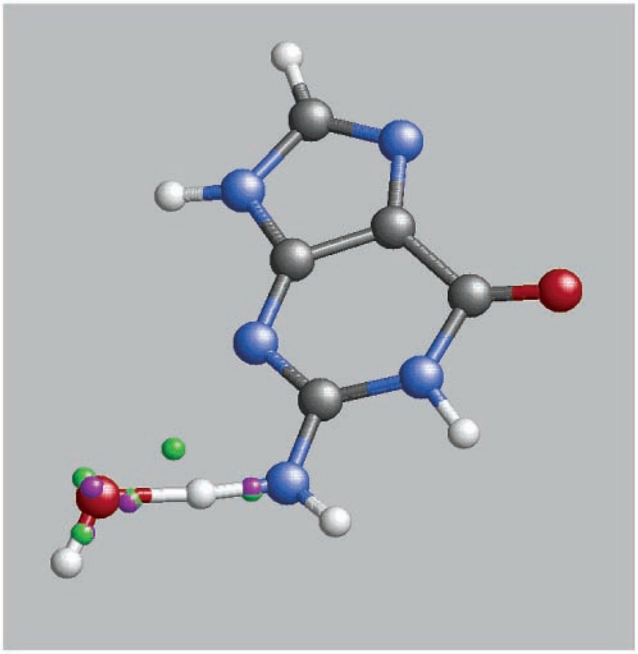

Figure 5. Halfway along the reaction path for the hydrogen abstraction leading to the formation of the guanine radical. Color coding is the same as in Figure 4. As in Figure 4, the transition state is the removal of a neutral hydrogen atom from the guanine (white sphere + green sphere). Again, note that the electron density in N2−H sigma bond is still present (overlapping green and magenta spheres near N2). From this angle it is also possible to see the spin-polarized lone pair on the oxygen.

the point on the reaction trajectory where the hydrogen is moving from the N2 site to the OH radical. Just as seen for the N9 dehydrogenation, the hydrogen transfer is concerted with the loss of electron density in the guanine conjugated rings.

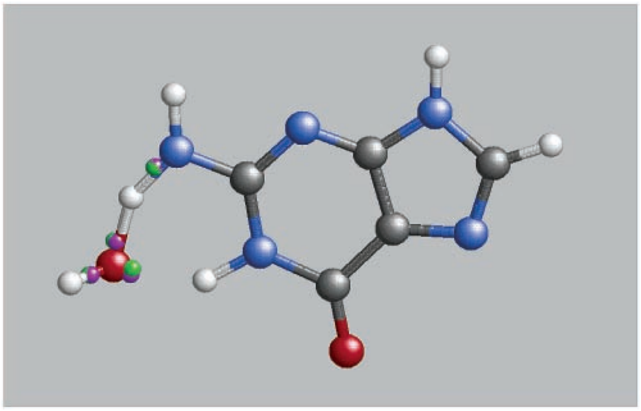

Figure 6. Halfway along the reaction path for the proton abstraction leading to the formation of a guanine radical. Color coding is the same as in Figure 4. In contrast to the mechanisms shown in Figures 4 and 5, the reaction proceeds with the removal of a proton from the guanine (white sphere). One can also see the overlapping green and magenta spheres on the oxygen—one of which give rise to the observed partial charge transfer (see Figure 9). Note that the electron density in N2−H *σ*-bond is still present (overlapping green and magenta spheres near N2). From this angle it is also possible to see the spin-polarized lone pair on the oxygen.

N1 Dehydrogenation. Last, we examine the reactions that can occur with the OH radical configured for N1 dehydrogenation, which we found to have the most complex reaction path for any of the sites studied. Starting from initial conditions as shown in Figure 3, in our initial simulation we found that the OH radical instead abstracted the hydrogen from N2. Thus, continuous dynamics from the initially prepared state shown in Figure 3 does not lead to spontaneous dehydrogenation of N1, but rather of N2. The actual mechanism suggested by WC analysis is that the initial OH radical attack at N1 abstracts a partial electron charge from the guanine conjugated ring, followed by the spontaneous removal of a proton from the N2 site (see Figure 6). A more detailed examination of this mechanism is discussed below.

C8 Hydroxylation. Experimental results indicate that hydroxyl radical addition to unsaturated carbon sites in guanine form stable intermediates.[17−19] In light of these findings in the context of our previous result on C8 dehydrogenation, we examine the energetics of OH radical addition to the C8 site. Indeed, in agreement with a previous study we find this radical to be stable, and its formation to be exothermic.[9] To facilitate the OH radical addition, we performed a constrained geometry optimization of the OH radical 2 Å above the guanine, in contrast to the dehydrogenation reactions which did not require that the initial state be optimized with respect to geometry. This observation indicates that it is likely the guanine must take on a particular conformation before this channel is reactive. Figure 7 shows the WC analysis of the configuration halfway along the reaction path. The electron from the guanine molecule is abstracted from the neighboring *π*-bond as expected.

C4 Hydroxylation. Experiments also point to the possibility of OH radical addition to the C4 site on guanine. We also find this radical to be stable, and its formation to be exothermic. Again, to facilitate the OH radical addition, we performed a constrained geometry optimization of the OH radical roughly 2 Å above the guanine. Figure 8 shows the WC analysis of the configuration halfway along the reaction path. The electron from the guanine molecule is abstracted from the neighboring carbon−carbon *π*-bond as expected. The resulting radical was run an additional picosecond beyond the reaction to see if there was a propensity to dissociate into water and a guanine radical

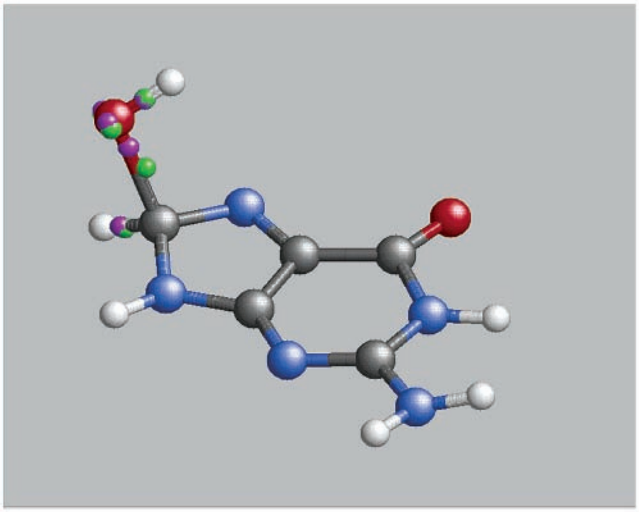

Figure 7. Halfway along the reaction path of the addition of the OH radical to guanine. Color coding is the same as in Figure 4. Note that the electron density in C8−H σ-bond is still present (overlapping green and magenta spheres). From this angle it is also possible to see the spin-polarized lone pair on the oxygen.

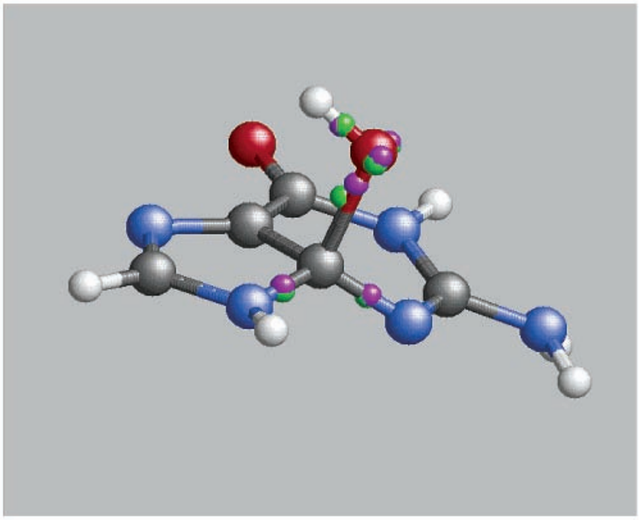

Figure 8. Halfway along the reaction path of the addition of the OH radical to the C4 on guanine. Color coding is the same as in Figure 4. Note that the electron density in both C4−N σ-bonds is still present (overlapping green and magenta spheres). From this angle it is also possible to see the spin-polarized lone pair on the oxygen.

cation as proposed in a recent experiment.[19] We did not observe any propensity to spontaneously form water and a guanine cation in the gas phase through the C4-hydroxylated intermediate.

In investigating whether this quasi-two-step mechanism shown in Figure 6 is an artifact of the ficticious mass of the Car-Parrinello electrons we reoptimized the wave function of this configuration to ensure that we are indeed on the Born-Oppenhiemer surface and examine the electronic structure both within CPMD and using static quantum chemical calculations. These calculations shed more light on the electronic structure of the system just after the OH closest approach to an N2 hydrogen. The NPA charges obtained from the quantum chemical calculations are consistent with the WC analysis that some electron transfer to the OH occurs during the interaction with N2. The NPA charge on the OH group at this point is $-0.67e^-$, compared with nearly zero at the initial structure of the CPMD simulation. Thus, the NPA results are very similar to the picture of the electronic mechanism given by the WCs.

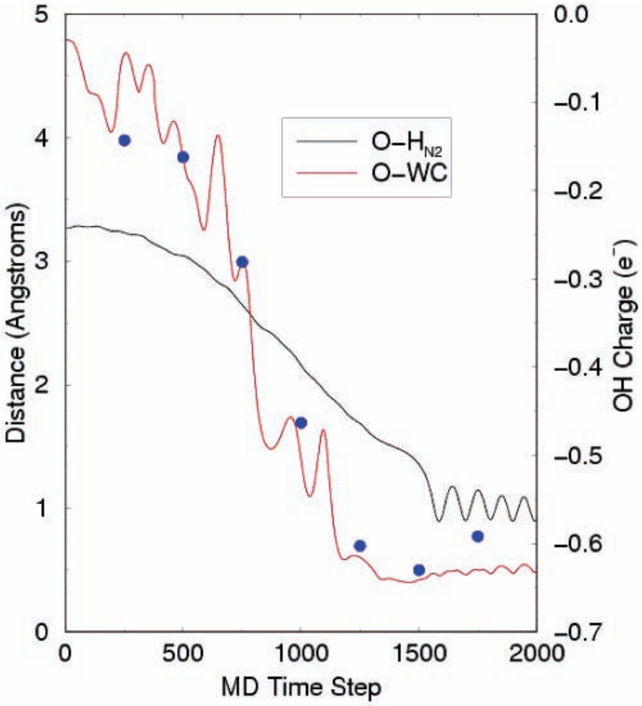

Figure 9. The simultaneous evolution of the distance of the H_{N2} proton and reacting WC to the radical oxygen. It is clear from the red curve that the WC is indeed located at the radical oxygen giving a net negative charge to the OH radical. The blue curve denotes the NPA charges computed for the precise configurations along the continuous trajectory. The NPA tracks well with the WC indicating that indeed charge is transferred to the OH radical during the chemical reaction. Each time step corresponds to 0.12 femtoseconds.

Although the WC for the electron transferred is located near the oxygen, its spatial extent is double that of a typical lone-pair Wannier function spread found in calculations performed on an isolated water molecule;[31,44] thus giving rise to an effective charge that should differ from $-1e^-$.

Upon initiating the CPMD from this reoptimized structure described above we find spontaneous abstraction of the proton from the N1 site. Given that the continuous trajectory starting from Figure 3 yields a different guanine radical than that arising from the aforementioned requenched configuration where the OH makes its closest approach leads one to conclude that initial conditions play an important role in determining the predicted products. Moreover, as we have seen N2-dehydrogenation occur in a more concerted electron and proton transfer (see Figure 5), it is clear that the amount of partial electron transfer at the transition state is highly dependent on initial conditions as well.

We further analyzed the mechanism of the hydrogen abstraction at the N2 position by calculating natural atomic orbital-based atomic charges at specific points of the original continuous trajectory. We then superimpose this plot on the N2 hydrogen-radical distance and the transferred WC-oxygen distance curves. The resulting plot is shown in Figure 9. Ones attention should first turn to the red and black curves. It is clear from these curves that the reacting electron (or WC) has shifted to the oxygen before the abstraction of the N2-proton. This supports a mechanism in which a portion of electron charge has transferred to the OH preceding the proton shift to form the final products of a guanine radical and water. This mechanism reflects the propensity for complete electron transfer to the OH in the condensed phase (see reactions 3 and 4 in Figure 2). It is evident from this curve that the NPA charges, denoted by the blue circles, track with the WC very well. This result corroborates

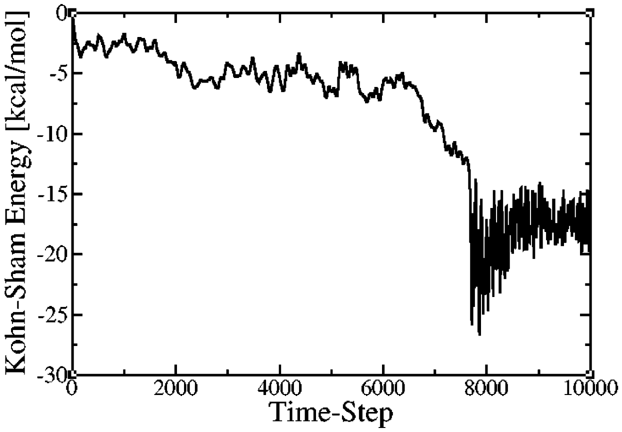

Figure 10. The Kohn−Sham energy as a function of time during the reacting trajectory corresponding to N2-dehydrogenation.

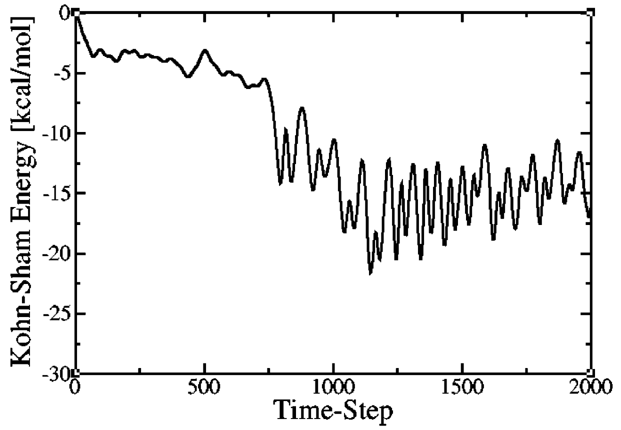

Figure 11. The Kohn−Sham energy as a function of time during the reacting trajectory corresponding to N9-dehydrogenation.

the WC picture and strongly indicates that the observed mechanism is not an artifact of the Boys criteria used in calculating the WCs or the plane-wave basis set. Moreover, we feel that this mechanism is reflective of most reaction channels in guanine-OH radical chemistry; namely, the degree to which the electron is transferred before the proton is abstracted to the OH moiety is highly dependent on initial conditions.

It is interesting to comment on the comparison of the reaction enthalpies calculated from CPMD and the Gaussian basis set calculations. As stated earlier, Table 2 denotes the reaction enthalpies obtained by separately optimizing the geometries of the individual reactants and products. It is important to realize that the static calculations assume *infinite* separation between the reactants and products when the enthalpies are computed. This is not the case with the CPMD calculations. In the CPMD calculations, the individual components of the reactants and products are free to interact. Thus, the absolute enthalpies from the CPMD calculations cannot be directly compared in a meaningful way to those obtained via the static calculations. For example, although there is agreement between the N2 hydrogen abstraction enthalpy (−26.98 kcal/mol) with the static calculation, the CPMD enthalpy obtained from the N9 hydrogen abstraction (−21 kcal/mol) is seemingly less exothermic (see Figures 10 and 11). This is attributed to a difference in the preparation of the initial and final states in the CPMD and static calculations rather than a fundamental disagreement of the two methods. The same is true for the C8 and C4 hydroxlyation reactions. Here, the initial states were prepared with the OH radical roughly 2 Å from the addition site. With this being said, it is clear that the CPMD trajectories *do* provide a meaningful description of the reaction dynamics as is evident from our analysis leading to Figure 9.

Conclusions

In this study we performed a detailed analysis of the possible mechanisms arising from guanine interacting with an OH radical using both Gaussian basis set density functional theory and CPMD. The unique feature of this study lies in the use of both static and dynamical quantum mechanical methods and state-of-the-art analysis in order to separately track the nuclear and electronic rearrangement during the dehydrogenation and hydroxylation reactions. Our results indicate that for all starting configurations in the plane of the guanine molecule (see Figure 3) *except* for the OH positioned in front of the C8 hydrogen, there is spontaneous dehydrogenation leading to the formation of a guanine radical and water. We also observe spontaneous dehydrogenation from an initial configuration lying perpendicular to the plane of the guanine molecule. Spontaneous hydroxylation at the C8 position is observed only after a geometry optimization is performed on the initial configuration. Our results are consistent within two different electronic structure packages and levels of theory. Certainly, the conditions of the present study cannot be mapped to experimental conditions in a unique fashion. It is clear from the experimental literature that the formation of a neutral guanine radical is also observed as a stable intermediate in the oxidation of guanine.[15,16,19,22] Thus, our results can be put into the context of the current knowledge in that we see *both* spontaneous dehydrogenation and hydroxylation in the initial stage of guanine oxidation with dehydrogenation free energetically favored. We feel that this is an important observation given recent experimental findings and proposed mechanisms. Moreover, within the dynamical framework used in this study we can discern between different levels of a concerted proton and electron transfer. WC and NPA analysis of the electron distributions during the dehydrogenation reactions suggest that in some configurations the transfer of an electron from the guanine to the OH radical precedes the shift of the hydrogen nucleus—an observation that would not have been possible without the explicit ab initio dynamics of the guanine and OH radical. Future directions of research will focus on using CPMD in conjunction with traditional quantum chemical methods to examine the oxidation of the other DNA bases and compare to the wealth of literature on this subject. One caveat of this study is that it was performed in the gas phase. Most likely there will be a reordering of some of the reaction energetics in water. To this end, we plan to initiate a more comprehensive CPMD study of the reaction of radiolysis products of DNA bases in aqueous conditions.

Acknowledgment. The authors thank Dr. Christine Hartman-Siantar for many helpful scientific discussions. One of us (C.J.M.) gratefully acknowledges useful conversations with Profs. U. Roethlisberger, J. Hutter, M. Parrinello, and J. A. Camarero. We also thank Prof. B. P. Mundy for a critical reading of this manuscript. This work was performed under the auspices of the U.S. Department of Energy by Lawrence Livermore National Laboratory under Contract W-7405-ENG-48 and was funded by the Laboratory Directed Research and Development Program at Lawrence Livermore National Laboratory (LLNL).

References and Notes

(1) Moiseenko, V. V.; Hamm, R. N.; Waker, A. J.; Prestwich, W. V. *Int. J. Radiat. Biol.* **1998**, *74*, 533−550.

(2) Nikjoo, H.; Oneill, P.; Goodhead, D. T.; Terrissol, M. *Int. J. Radiat. Biol.* **1997**, *71*, 467−483.

(3) Chatterjee, A.; Holley, W. R. *Int. J. Quantum Chem.* **1991**, *39*, 709−727.

(4) *Advances in cell aging and gerontology*; Elsevier: New York, 2001; Vol. 4.

(5) Close, D. M. *Radiat. Res.* **1993**, *135*, 1.

(6) Sagstuen, E.; Hole, E. O.; Nelson, W. H.; Close, D. M. *Radiat. Res.* **1996**, *146*, 425.

(7) Sagstuen, E.; Hole, E. O.; Nelson, W. H.; Close, D. M. *Radiat. Res.* **1998**, *149*, 120.

(8) Close, D. M.; Eriksson, L. A.; Hole, E. O.; Sagstuen, E.; Nelson, W. H. *J. Phys. Chem. B* **2000**, *104*, 9343−9350.

(9) Wetmore, S. D.; Boyd, R. J.; Eriksson, L. A. *J. Phys. Chem. B* **1998**, *102*, 9332−9343.

(10) Wetmore, S. D.; Boyd, R. J.; Eriksson, L. A. *J. Phys. Chem. B* **1998**, *102*, 5369−5377.

(11) Wetmore, S. D.; Himo, F.; Boyd, R. J.; Eriksson, L. A. *J. Phys. Chem. B* **1998**, *102*, 7484−7491.

(12) Wetmore, S. D.; Boyd, R. J.; Himo, F.; Eriksson, L. A. *J. Phys. Chem. B* **1999**, *103*, 3051−3052.

(13) Wetmore, S. D.; Boyd, R. J.; Eriksson, L. A. *Chem. Phys. Lett.* **2000**, *322*, 129−135.

(14) Steenken, S.; Jovanovic, S. V. *J. Am. Chem. Soc.* **1997**, *119*, 617−618.

(15) Vialas, C.; Pratviel, G.; Claparols, C.; Meunier, B. *J. Am. Chem. Soc.* **1998**, *120*, 11548−11553.

(16) Yoshioka, Y.; Kitagawa, Y.; Takano, Y.; Yamaguchi, K.; Nakamura, T.; Saito, I. *J. Am. Chem. Soc.* **1999**, *121*, 8712−8719.

(17) Cadet, J.; Delatour, T.; Douki, T.; Gasparutto, D.; Pouget, J. P.; Ravanat, J. L.; Sauvaigo, S. *Mutat. Res.−Fundam. Mol. Mech. Mutat*. **1999**, *424*, 9−21.

(18) Bamatraf, M. M. M.; O'Neill, P.; Rao, B. S. M. *J. Phys. Chem. B* **2000**, *104*, 636−642.

(19) Candeias, L. P.; Steenken, S. *Chem.−Eur. J.* **2000**, *6*, 475−484.

(20) Kuzmin, V. A.; Dourandin, A.; Shafirovich, V.; Geacintov, N. E. *Phys. Chem. Chem. Phys.* **2000**, *2*, 1531−1535.

(21) Chworos, A.; Coppel, Y.; Dubey, I.; Pratviel, G.; Meunier, B. *J. Am. Chem. Soc.* **2001**, *123*, 5867−5877.

(22) Weatherly, S. C.; Yang, I. V.; Thorp, H. H. *J. Am. Chem. Soc.* **2001**, *123*, 1236−1237.

(23) Baik, M. H.; Silverman, J. S.; Yang, I. V.; Ropp, P. A.; Szalai, V. A.; Yang, W. T.; Thorp, H. H. *J. Phys. Chem. B* **2001**, *105*, 6437−6444.

(24) Prat, F.; Houk, K. N.; Foote, C. S. *J. Am. Chem. Soc.* **1998**, *120*, 845−846.

(25) Car, R.; Parrinello, M. *Phys. Rev. Lett.* **1985**, *55*, 2471−2474.

(26) Hutter, J.; Ballone, P.; Bernasconi, M.; Focher, P.; Fois, E.; Goedecker, S.; Parrinello, M.; Tuckerman, M. E. *CPMD code, version 3.3*; MPI fuer Festkoerperforschung, Stuttgart IBM Zurich Research Laboratory, 1990−1996.

(27) Kohn, W.; Sham, L. A. *Phys. Rev. A* **1965**, *140*, 1133.

(28) Sprik, M.; Hutter, J.; Parrinello, M. *J. Chem. Phys.* **1996**, *105*, 1142−1152.

(29) Marzari, N.; Vanderbilt, D. *Phys. Rev. B: Condens. Matter* **1997**, *56*, 12847−12865.

(30) Silvestrelli, P. L.; Marzari, N.; Vanderbilt, D.; Parrinello, M. *Solid State Commun.* **1998**, *107*, 7−11.

(31) Berghold, G.; Mundy, C. J.; Romero, A. H.; Hutter, J.; Parrinello, M. *Phys. Rev. B* **2000**, *61*, 10040−10048.

(32) Boys, S. F. *Rev. Mod. Phys.* **1960**, *32*, 296.

(33) Mundy, C. J.; Hutter, J.; Parrinello, M. *J. Am. Chem. Soc.* **2000**, *122*, 4837−4838.

(34) Mercuri, F.; Mundy, C. J.; Parrinello, M. *J. Phys. Chem. A* **2001**, *105*, 8423−8427.

(35) Becke, A. D. *Phys. Rev. A, Gen. Phys. (USA)* **1988**, *38*, 3098−3100.

(36) Lee, C. T.; Yang, W. T.; Parr, R. G. *Phys. Rev. B, Condens. Matter (USA)* **1988**, *37*, 785−789.

(37) Hartwigsen, C.; Goedecker, S.; Hutter, J. *Phys. Rev. B−Condens. Matter* **1998**, *58*, 3641−3662.

(38) Martyna, G. J.; Tuckerman, M. E. *J. Chem. Phys.* **1999**, *110*, 2810−2821.

(39) Becke, A. D. *J. Chem. Phys.* **1993**, *98*, 5648−5652.

(40) Reed, A. E.; Weinstock, R. B.; Weinhold, F. *J. Chem. Phys.* **1985**, *83*, 735−746.

(41) Barone, V.; Cossi, M. *J. Phys. Chem. A* **1998**, *102*, 1995−2001.

(42) Frisch, M. J.; Trucks, G. W.; Schlegel, H. B.; Scuseria, G. E.; Robb, M. A.; Cheeseman, J. R.; Zakrzewski, V. G.; Montgomery, J. A., Jr.; Stratmann, R. E.; Burant, J. C.; Dapprich, S.; Millam, J. M.; Daniels, A. D.; Kudin, K. N.; Strain, M. C.; Farkas, O.; Tomasi, J.; Barone, V.; Cossi, M.; Cammi, R.; Mennucci, B.; Pomelli, C.; Adamo, C.; Clifford, S.; Ochterski, J.; Petersson, G. A.; Ayala, P. Y.; Cui, Q.; Morokuma, K.; Malick, D. K.; Rabuck, A. D.; Raghavachari, K.; Foresman, J. B.; Cioslowski, J.; Ortiz, J. V.; Stefanov, B. B.; Liu, G.; Liashenko, A.; Piskorz, P.; Komaromi, I.; Gomperts, R.; Martin, R. L.; Fox, D. J.; Keith, T.; Al-Laham, M. A.; Peng, C. Y.; Nanayakkara, A.; Gonzalez, C.; Challacombe, M. W.; Gill, P. M. W.; Johnson, B.; Chen, W.; Wong, M. W.; Andres, J. L.; Gonzalez, C.; Head-Gordon, M.; Replogle, E. S.; Pople, J. A.; *Gaussian 98*, A.4.; Gaussian Inc.: Pittsburgh, PA, 1998.

(43) Douki, T.; Spinelli, S.; Ravanat, J. L.; Cadet, J. *J. Chem. Soc., Perkin Trans. 2* **1999**, 1875−1880.

(44) Silvestrelli, P. L.; Parrinello, M. *Phys. Rev. Lett.* **1999**, *82*, 5415.

(45) Dougherty, D.; Younathan, E. S.; Voll, R.; Abdulnur, S.; McGlynn, S. P. *J. Electron Spectrosc. Relat. Phenom.* **1978**, *13*, 379−393.

(46) Schluz, P. A.; Mead, R. D.; Jones, P. L.; Lineberger, W. C. *J. Chem. Phys.* **1982**, *77*, 1153−1165.